Ferromagnetic states in Fe-Ru systems studied by *ab initio* calculation and ion-beam mixing

Xiang He, Wen-Chao Wang, and Bai-Xin Liu*

Advanced Materials Laboratory, Department of Materials Science and Engineering, Tsinghua University, Beijing 100084, China

(Received 30 May 2007; revised manuscript received 1 August 2007; published 2 January 2008)

Ab initio calculations reveal that Fe_3Ru alloys of the $D0_3$, $A15$, and $D0_{22}$ structures will behave as ferromagnets. Moreover, $Fe_{50}Ru_{50}$ alloys of $L2_a$, $B2$, and α-NiAs structures will also behave ferromagnetically. In ion-beam-mixing experiments, a magnetic $Fe_{50}Ru_{50}$ alloy of $B2$, i.e., bcc, structure is obtained at a dose of 1×10^{15} Xe^+/cm^2. Interestingly, a nonmagnetic $Fe_{50}Ru_{50}$ alloy of $L1_0$, i.e., fcc, structure is also obtained under the same conditions and the predictions are in agreement with observations obtained from ion-beam-mixing experiments and magnetism measurements.

DOI: 10.1103/PhysRevB.77.012401 PACS number(s): 75.75.+a, 76.50.+g

The effect of impurities of 3*d* and 4*d* transition metals in Fe has been a long-standing research subject. Concerning the magnetic behaviors of these alloys in the equilibrium states, researchers have frequently concentrated on studying the Fe-Ru alloys because Ru is one of the elements that scarcely decrease the average magnetic moment of the alloys.[1] Nonetheless, the structure and magnetic properties of the Fe-Ru alloys have not yet been experimentally and theoretically studied in detail, probably because only the hcp alloy is easily formed in the Fe-Ru system under equilibrium conditions, and this alloy is always antiferromagnetic.[2,3] Recently, some researchers have shown that addition of Ru into some Fe-based alloys may enhance anticorrosion, wear resistance, and thermal stability without reduction of the average magnetic moment.[4,5] It is therefore of both practical and theoretical importance to pursue a thorough investigation of the Fe-Ru system concerning the metastable phase formation, magnetic properties, and associated underlying physics to reach a better understanding of the related issues.

To perform *ab initio* calculations, we employed the Vienna *ab initio* simulation package (VASP),[6–8] in which the projected augmented wave (PAW) pseudopotentials have been constructed by considering the all-electron effect. The exchange and correlation effects were described by the functional proposed by Perdew and Zunger,[9] employing generalized gradient approximation (GGA) corrections.[10] Brillouin-zone integrations were performed using an $11\times11\times11$ Monkhorst-Pack[11] grid leading to 56 irreducible *k* points. The plane-wave cutoff energy was set to be 267.9 eV. In addition, the Vosko-Wilk-Nusair interpolations were used for the correlation part of the exchange correlation functional.[12] In the calculations, we first set the coordinates of the atoms in the INCAR file, which is the central input file of VASP, according to the structure, and then set different lattice constants to calculate the energy of the possible metastable phases. After calculations, we fitted the results to the Murnaghan equation of states to determine the lattice constant and minimum energy of the structure.

It is known that there are a lot of different structures for the A_3B, AB_3, and AB phases. The choice of the possible structures in *ab initio* calculations is based on the following considerations.

First, of all the possible structures, some are very complicated, e.g., the $D0_2$ and $D0_{21}$ structures are composed of more than 16 atoms per unit cell. The $L1_a$ structure can also be considered complicated, as it has 32 atoms per unit cell. These complicated structures certainly require highly sufficient kinetic conditions to nucleate and grow, e.g., a relatively high temperature to enhance the atomic mobility as well as a long time to enable the atoms to organize themselves into an ordered configuration. In other words, if such kinetic conditions are not available, these structures can scarcely be formed.

Second, the nonequilibrium or metastable crystalline phases that have so far been produced by nonequilibrium processing techniques, e.g., solid-state interfacial reaction and/or ion-beam mixing, were only of simple structures, such as hcp, bcc, and fcc structures, but not any kind of complicated structures, probably because of the restricted kinetic conditions involved in the production processes.

In the experimental study, we applied the method of ion-beam mixing (IBM), which is conducted in two steps, i.e., first preparation of the metal-metal multilayers; and second, ion irradiation of the multilayers. The detailed description of IBM can be found in the literature.[13] In the present IBM experiment, 200 keV Xe^+ ions were applied as the irradiating ions. Three sets of Fe-Ru multilayered samples were designed with overall compositions of $Fe_{75}Ru_{25}$, $Fe_{50}Ru_{50}$, and $Fe_{25}Ru_{75}$, respectively. The total thickness of the Fe-Ru multilayered samples is about 40 nm, designed to match the TRIM code calculated projected range plus projected range straggling of 200 keV Xe^+ ions. The Fe-Ru multilayered samples were prepared by depositing alternately pure Fe (99.9%) and Ru (99.9%) at a rate of 0.5 Å/s onto NaCl single crystal substrates in an *e*-gun evaporation system with a vacuum level of 10^{-6} Pa. The designed overall compositions of the Fe-Ru multilayered samples can be achieved by adjusting the relative thicknesses of the Fe and Ru layers. The as-deposited Fe-Ru multilayered samples were then irradiated by 200 keV Xe^+ ions in an implanter with a vacuum level better than 5×10^{-4} Pa; irradiation doses were in the range from 6×10^{14} to 9×10^{15} Xe^+/cm^2. The sample holder is cooled by liquid nitrogen (77 K) during the irradiation, and the xenon ion current density is confined to be about 2 $\mu A/cm^2$ to minimize heating effects. For structural characterization, all the Fe-Ru multilayered samples were removed from the substrates in deionized water and put onto Cu grids for bright field examination and selected area diffraction (SAD) analysis at room temperature by transmission electron microscopy. For determination of the composition of

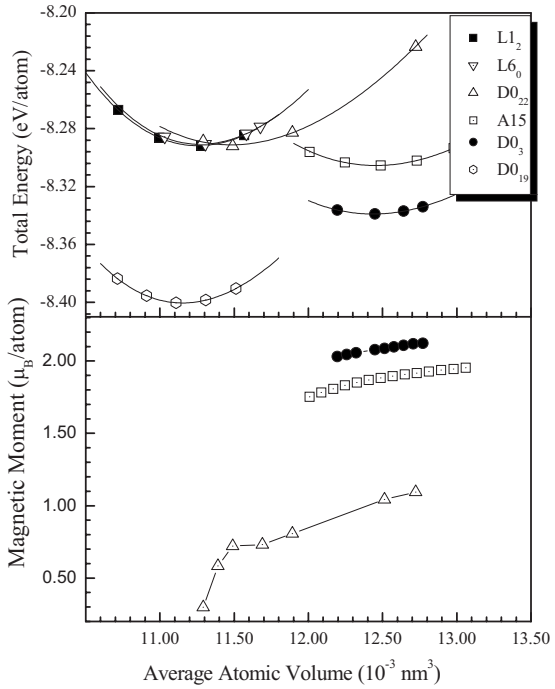

FIG. 1. Correlation of total energies (upper panel) and magnetic moments (lower panel) against the lattice constant of $Fe_{75}Ru_{25}$ obtained by *ab initio* calculations within the GGA.

the as-deposited Fe-Ru multilayered samples and the resultant alloy phases, energy-dispersive spectroscopy was employed and the measuring error was about 5%. An alternating gradient magnetometer was used to identify the magnetic moment of the samples and a PLASMA-SPEC-I inductively coupled plasma atomic emission spectrum was employed to determine the exact quantity of Fe atoms in the alloys of interest.[14]

It is known that IBM is a process far from equilibrium and can generally be divided into two steps,[15] i.e., an atomic collision cascade triggered by the impinging ions, followed by a relaxation period. In the present study, the 200 keV xenon ions triggered the atomic collision cascade, which was responsible for inducing atomic mixing between the Fe and Ru layers in the as-deposited Fe-Ru multilayered samples. After receiving an adequate ion dose, the Fe and Ru atoms were uniformly mixed, and the mixture was most likely in a highly energetic and disordered state. According to the atomic collision theory, the relaxation period is extremely short, which allows only a limited rearrangement of the atoms in the Fe-Ru mixture. Consequently, upon relaxation, the highly energetic and disordered Fe-Ru mixture could reside in one of the possible intermediate states of lower energy, resulting in forming some Fe-Ru metastable alloys that are not obtainable under equilibrium conditions. The ion-mixed Fe-Ru metastable alloys were then used to study the related magnetic properties.

We first calculate the energy and magnetic moment vs volume correlation of the Fe_3Ru alloy and then fit it to the Murnaghan equation of states[16] to obtain its cohesive properties. The calculated results are shown in Fig. 1 and listed in Table I. From Fig. 1 and Table I one sees that the increasing order of structural stability for the possible $Fe_{75}Ru_{25}$ phase is $D0_{19}$, $D0_3$, $A15$, $D0_{22}$, $L6_0$, and $L1_2$ and that the six calculated structures can be divided into two groups according to the calculated heats of formation listed in Table I. In the first group, the heats of formation of the $D0_{22}$, $L6_0$, and $L1_2$ structures are quite close to each other. In the second group, the heats of formation of $A15$, $D0_3$, and $D0_{19}$ structures are a little lower than those in the first group. One can see from the calculated results that the $D0_{19}$ structure is the most likely one to be formed and it is nonmagnetic. The calculated results are in good agreement with those of previous studies

TABLE I. Cohesion properties of Fe_3Ru and $Fe_{50}Ru_{50}$ alloys in different structures obtained from the present *ab initio* calculations. E_{min} is the minimum total energy; ΔH the heat of formation; V_0 the equilibrium average atomic volume; a the lattice constant; c/a the relaxed c/a ratio; and M the magnetic moment of Ni at the equilibrium volume.

	a (Å)	c/a	V (Å^3/atom)	E_{min} (eV/atom)	ΔH (eV/atom)	M (μ_B)
			Fe_3Ru			
$D0_{19}$	5.02	0.786	11.17	−8.400	0.05	
$D0_3$	5.84		12.45	−8.339	0.11	2.07
$A15$	4.63		12.41	−8.305	0.15	1.87
$D0_{22}$	3.47	2.058	11.49	−8.292	0.16	0.7
$L1_2$	3.56		11.28	−8.292	0.16	
$L6_0$	3.69 (3.63)	0.999	11.31	−8.290	0.16	
			$Fe_{50}Ru_{50}$			
$L1_0$	3.67 (3.62)	0.985	12.11	−8.513	0.18	
$L2_a$	3.01	1.001	13.09	−8.500	0.19	1.62
B2	2.96 (2.69)		12.97	−8.494	0.20	1.53 (0.9)
α-NiAs	3.60	1.226	14.04	−7.985	0.70	0.93
$B1$	4.78		13.65	−7.696	0.99	

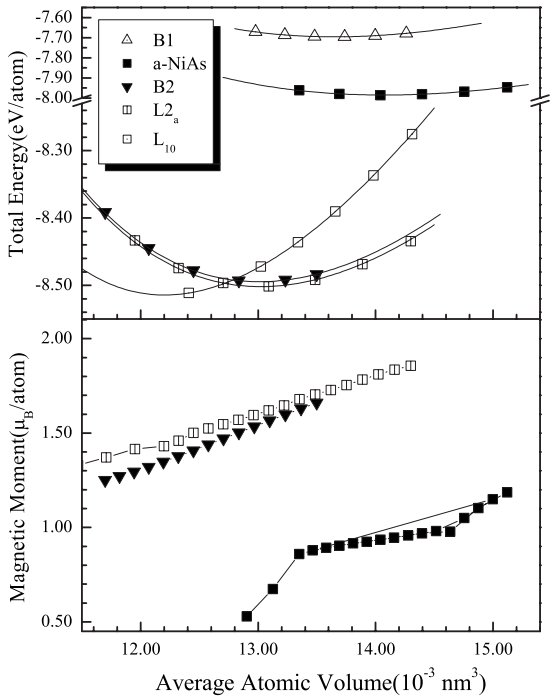

FIG. 2. Correlation of total energies (upper panel) and magnetic moments (lower panel) against the lattice constant of $Fe_{50}Ru_{50}$ obtained by *ab initio* calculations within the GGA.

and experiments.[2,3,17] In addition, the $D0_3$, $A15$, and $D0_{22}$ structures all behave ferromagnetically and the magnetic moments are $2.07\mu_B$, $1.87\mu_B$, and $0.7\mu_B$, respectively.

We then perform similar calculations to study the structural stability and magnetic properties of $Fe_{50}Ru_{50}$ and $Fe_{25}Ru_{75}$ in their metastable states. Table I lists the fitted cohesive properties, and Fig. 2 shows the correlations of the total energies and magnetic moments against the average atomic volume of $Fe_{50}Ru_{50}$. One sees that $Fe_{25}Ru_{75}$ has a similar situation to $Fe_{75}Ru_{25}$. The $D0_{19}$ structure has the lowest heat of formation and therefore is the most likely phase to be formed. Nonetheless, all the possible structures calculated are nonmagnetic. We therefore focus on studying $Fe_{50}Ru_{50}$. It can easily be seen from Fig. 2 and Table I that the $L1_0$, $B2$, and $L2_a$ structures are at the same energy level, which is much lower than that of the $B1$ and α-NiAs structures, indicating that these structures are easily formed, and that the $L2_a$, $B2$, and α-NiAs structures all behave ferromagnetically and their magnetic moments are $1.62\mu_B$, $1.53\mu_B$, and $0.93\mu_B$, respectively. Interestingly, although the $L1_0$, $B2$, and $L2_a$ structures are at the same energy level, the $B2$ and $L2_a$ structures are ferromagnetic, yet the $L1_0$ structure is not.

In the experimental study, we first identified the structures of three sets of as-deposited Fe-Ru multilayered samples by SAD analysis. It turned out that all the as-deposited Fe-Ru multilayered samples consist of polycrystalline Fe and Ru structures. Upon ion irradiation, some interesting structural phase transitions were observed and are described in detail in the following. In the $Fe_{75}Ru_{25}$ sample, a fcc phase (a =3.63 Å) was formed at a dose of 3×10^{15} Xe^+/cm^2. For the $Fe_{50}Ru_{50}$ sample, a structural phase transition was observed, i.e., a fcc phase (a=3.62 Å) and a bcc phase (a=2.69 Å)

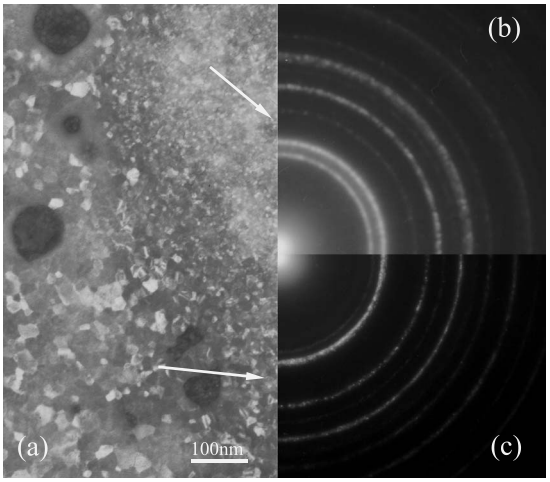

FIG. 3. (a) Bright field image of $Fe_{50}Ru_{50}$ sample at the irradiation dose of 1×10^{15} Xe^+/cm^2; (b) SAD pattern of area I; (c) SAD pattern of area II.

were formed at a dose of 1×10^{15} Xe^+/cm^2. The SAD patterns and the bright field images of the above fcc and bcc phases are shown in Fig. 3. Moreover, the measured magnetic moment of the bcc structure is $0.9\mu_B$, whereas the fcc structure is nonferromagnetic. The magnetic hysteresis loop is shown in Fig. 4. For the $Fe_{25}Ru_{75}$ sample, however, no interesting structural phase transition was found upon ion irradiation. Figures 5 and 6 show the SAD pattern and the corresponding magnetization curve obtained at room temperature for the $Fe_{25}Ru_{75}$ sample at an irradiation dose of 1×10^{15} Xe^+/cm^2. Obviously, $Fe_{25}Ru_{75}$ is nonferromagnetic.

It is of importance to compare the experimental results with the previous theoretical and experimental observations. First, for the $Fe_{75}Ru_{25}$ alloys, it is seen from Table I that the lattice constant of the $L6_0$ structure is 3.69 Å, which is quite compatible with the reported experimental observation (3.63 Å). Second, it is also seen from Table I that hcp $Fe_{75}Ru_{25}$ is predicted to be nonmagnetic, which is in accordance with previous experimental results.[2,3,17] Third, as it is

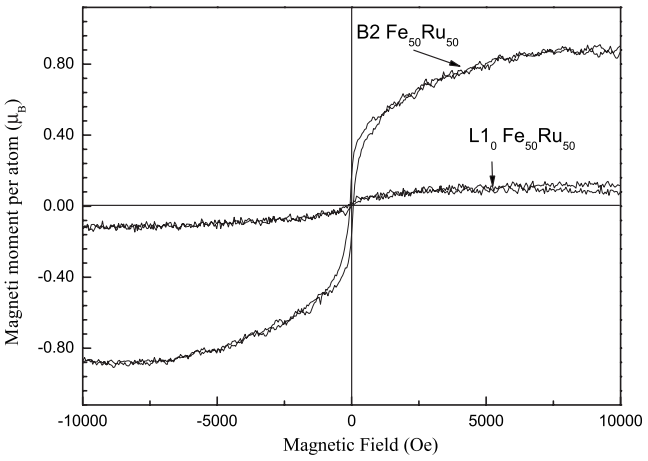

FIG. 4. Magnetization curves obtained at room temperature for the sample $Fe_{50}Ru_{50}$ at the irradiation dose of 1×10^{15} Xe^+/cm^2. The applied magnetic field was parallel to the sample.

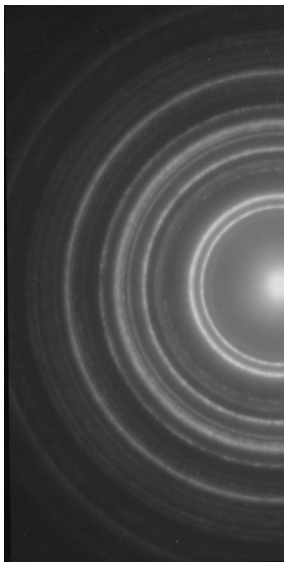

FIG. 5. SAD pattern of $Fe_{25}Ru_{75}$ sample at the irradiation dose of 1×10^{15} Xe^+/cm^2.

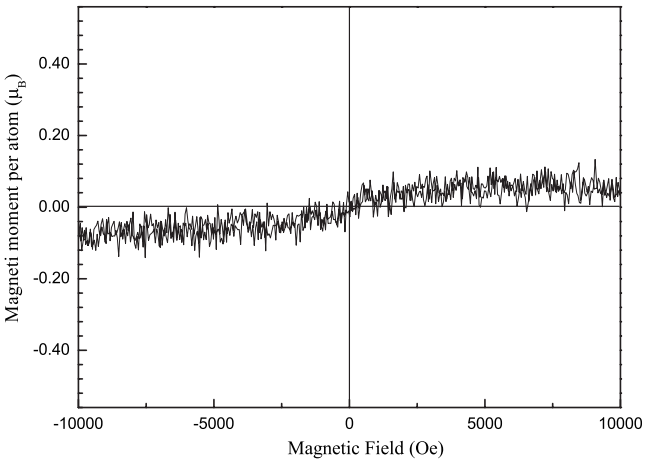

FIG. 6. Magnetization curve obtained at room temperature for the sample $Fe_{25}Ru_{75}$ at the irradiation dose of 1×10^{15} Xe^+/cm^2. The applied magnetic field was parallel to the sample.

seen from Table I and Fig. 2, for the $Fe_{50}Ru_{50}$ alloy, the lattice constant and magnetic moment of the B_2 structure are predicted to be $a=2.96$ Å and $1.53\mu_B$, matching well with the experimentally observed values of 2.69 Å and $0.9\mu_B$, respectively. In this respect, Kobayashi *et al.*[18] have reported that Ru in α-Fe became ferromagnetic due to the bcc structure, and Ru addition to Fe enhanced the magnetic moment at the Fe site because of the magnetovolume effect and large spin splitting at a Ru concentration of 20 at. %. It is noted that the magnetic moment of pure bcc Fe is $2.21\mu_B$,[19] and therefore the presently calculated magnetic moment ($1.53\mu_B$) of the $Fe_{50}Ru_{50}$ $B2$ structure is reasonable. Fourth, $L1_0$ $Fe_{50}Ru_{50}$ is predicted to behave nonmagnetically and the lattice constant is predicted to be $a=3.65$ Å, which is also in good accordance with the experimental observation ($a=3.62$ Å). From the calculation results, we find that the ground states of $Fe_{75}Ru_{25}$ and $Fe_{50}Ru_{50}$ are $D0_{19}$ and $L1_0$, respectively. Interestingly, the two structures are both close-packed structures, indicating that the close-packed structures are more stable than other structures in the Fe-Ru system. According to the present *ab initio* calculations as well as the results obtained by Kobayashi *et al.*, in the close-packed structures, the magnetovolume effect induced by the inclusion of the Ru atoms can be reduced and therefore the structures could behave nonmagnetically. Finally, $Fe_{25}Ru_{75}$ is calculated to be nonferromagnetic, which is also in good accordance with the experimental results.

In summary, we have shown that *ab initio* calculations predict and IBM experiments confirm the ferromagnetic states of the Fe-Ru system. In ion-beam-mixing experiments, a magnetic $B2$ $Fe_{50}Ru_{50}$ (bcc type) phase is indeed obtained, and interestingly a nonmagnetic $L1_0$ $Fe_{50}Ru_{50}$ (fcc type) phase is also formed under the same conditions, matching well with the prediction from the *ab initio* calculations.

The authors are grateful for financial support from the National Natural Science Foundation of China (Grant No. 50531040), The Ministry of Science and Technology of China (Grant No. 2006CB605201), and the Administration of Tsinghua University.

*Corresponding author. FAX: +86 10 6278 1255. dmslbx@tsinghua.edu.cn

[1] B. Drittler, N. Stefanou, S. Blugel, R. Zeller, and P. H. Dederichs, Phys. Rev. B **40**, 8203 (1989).
[2] D. I. C. Pearson and J. M. Williams, J. Phys. F: Met. Phys. **9**, 1797 (1979).
[3] Hong-Ju Moon, WonDong Kim, S. J. Oh, Jungwhan Park, J. G. Park, E. J. Cho, J. I. Lee, and H. C. Ri, J. Korean Phys. Soc. **36**, 49 (2000).
[4] K. Shiiki, Y. Shiroishi, N. Kumasaka, and S. Aoki, IEEE Trans. Magn. **MAG-4**, 493 (1985).
[5] K. Hayashi, M. Hayakawa, W. Ishikawa, Y. Ochiai, Y. Iwasaki, and K. Aso, J. Appl. Phys. **64**, 772 (1988).
[6] G. Kresse and J. Hafner, Phys. Rev. B **47**, 558 (1993).
[7] G. Kresse and J. Furthmüller, Comput. Mater. Sci. **6**, 15 (1996).
[8] G. Kresse and J. Furthmüller, Phys. Rev. B **54**, 11169 (1996).
[9] J. P. Perdew and A. Zunger, Phys. Rev. B **23**, 5048 (1981).
[10] J. P. Perdew, J. A. Chevary, S. H. Vosko, K. A. Jackson, M. R. Pederson, D. J. Singh, and C. Fiolhais, Phys. Rev. B **46**, 6671 (1992).
[11] H. J. Monkhorst and J. D. Pack, Phys. Rev. B **13**, 5188 (1976).
[12] S. H. Vosko, L. Wilk, and M. Nusair, Can. J. Phys. **58**, 1200 (1980).
[13] B. X. Liu, W. S. Lai, and Q. Zhang, Mater. Sci. Eng., R. **29**, 1 (2000).
[14] T. Yang, B. X. Liu, F. Pan, J. Luo, and K. Tao, J. Phys.: Condens. Matter **7**, 1121 (1995).
[15] B. X. Liu, W. S. Lai, and Z. J. Zhang, Adv. Phys. **50**, 367 (2001).
[16] J. P. Poirier, *Introduction to the Physics of the Earth's Interior* (Cambridge University Press, Cambridge, U.K., 1991).
[17] E. Raub and W. Plate, Z. Metallkd. **51**, 477 (1960).
[18] Mitsuru Kobayashi, Noriaki Ando, Tadashi Kai, Noriyuki Takano, and Kazuo Shiiki, J. Phys.: Condens. Matter **7**, 9607 (1995).
[19] L. T. Kong and B. X. Liu, Appl. Phys. Lett. **84**, 3627 (2004).